1-1-2020

Thresholds of mangrove survival under rapid sea level rise

N Saintilan

N Khan

E Ashe

Jeffrey Kelleway
University of Wollongong, jeffreyk@uow.edu.au

Kerrylee Rogers
University of Wollongong, kerrylee@uow.edu.au

See next page for additional authors

Thresholds of mangrove survival under rapid sea level rise

Abstract

Copyright © 2020 The Authors, some rights reserved; exclusive licensee American Association for the Advancement of Science. No claim to original U.S. Government Works. The response of mangroves to high rates of relative sea level rise (RSLR) is poorly understood. We explore the limits of mangrove vertical accretion to sustained periods of RSLR in the final stages of deglaciation. The timing of initiation and rate of mangrove vertical accretion were compared with independently modeled rates of RSLR for 78 locations. Mangrove forests expanded between 9800 and 7500 years ago, vertically accreting thick sequences of organic sediments at a rate principally driven by the rate of RSLR, representing an important carbon sink. We found it very likely (>90% probability) that mangroves were unable to initiate sustained accretion when RSLR rates exceeded 6.1 millimeters per year. This threshold is likely to be surpassed on tropical coastlines within 30 years under high-emissions scenarios.

Publication Details

Saintilan, N., Khan, N., Ashe, E., Kelleway, J., Rogers, K., Woodroffe, C. & Horton, B. (2020). Thresholds of mangrove survival under rapid sea level rise. Science, 368 (6495), 1118-1121.

Authors

N Saintilan, N Khan, E Ashe, Jeffrey Kelleway, Kerrylee Rogers, Colin D. Woodroffe, and B Horton

Title: *Thresholds of mangrove survival under rapid sea-level rise*

Authors: N. Saintilan[1*], N.S. Khan[2,3], E. Ashe[4], J.J. Kelleway[5], K. Rogers[5,6], C.D. Woodroffe[5], B.P. Horton [7,8]

Affiliations:

[1]Department of Earth and Environmental Sciences, Macquarie University, Australia.

[2]Department of Earth Sciences, University of Hong Kong, Hong Kong.

[3]Swire Marine Institute of Marine Science, University of Hong Kong, Hong Kong.

[4]Department of Earth and Planetary Sciences, Rutgers University, United States of America.

[5]School of Earth, Atmospheric and Life Sciences, University of Wollongong, Australia.

[6]Geoquest Research Centre, University of Wollongong, Australia

[7]Asian School of Environment, Nanyang Technological University, Singapore.

[8] Earth Observatory of Singapore, Nanyang Technological University, Singapore.

*Correspondence to: neil.saintilan@mq.edu.au

Abstract:

The response of mangroves to high rates of relative sea-level rise (RSLR) is poorly understood. We explore the limits of mangrove vertical accretion to sustained periods of RSLR in the final stages of deglaciation. The timing of initiation and rate of mangrove vertical accretion was compared to independently modelled rates of RSLR for 78 locations. Mangrove forests expanded between 9800 and 7500 years ago, vertically accreting thick sequences of organic secdiments at a rate principally driven by the rate of RSLR, representing an important carbon sink. We found it very likely (>90% probability) that mangroves were unable to initiate sustained accretion when RSLR rates exceeded 6.1 mm yr^{-1}. This threshold is likely to be surpassed on tropical coastlines within 30 years under high emissions scenarios.

One Sentence Summary: Mangrove response to sea-level rise in the final stages of deglaciation reveal thresholds possibly exceeded in the next 30 years

Main Text:

The rate of relative sea-level rise (RSLR) in tropical and subtropical locations is projected to accelerate from current trends of ~3.4 mm yr^{-1} to a mean estimate of ~5 mm yr^{-1} under low-emissions scenarios and ~10 mm yr^{-1} under high emissions scenarios by 2100 *(1,2)*. Modelling of feedbacks between RSLR, vertical accretion, root mass formation, and tidal marsh and mangrove vulnerability under sustained high rates of RSLR is vital for the survival of these ecologically and economically important coastal environments (*2*). Some tidal marshes have been projected to survive RSLR of over 10 mm yr^{-1} where supported by high available suspended sediment concentrations *(3)*, based on accretion data that span annual to decadal timescales. Reconstructions using paleoenvironmental proxies, however have suggested UK marshes were vulnerable to retreat at RSLR of 7 mm yr^{-1} (*4*).

Mangroves grow in sheltered intertidal environments that are exposed to the effects of RSLR *(5)*. They support among the highest rates of carbon burial of all ecosystems *(6)*, and a growing body of evidence suggests this efficiency is enhanced by RSLR *(7)*. However, empirical data on mangrove response to high rates of RSLR are lacking, given the limited observation period (1-16 years) of real-time measurements *(5)*.

Here we assess the mangrove response to RSLR from the paleorecord of mangrove vertical accretion preserved in the sedimentary archives of continental shelves and coastal lowlands. Mangrove forests have initiated and drowned in association with variability in the rate of RSLR following the onset of deglaciation ~26,000 to 20,000 years ago (8). Prior to the Holocene, long-term RSLR rates of >12mm yr^{-1} *(8)* exceeded the capacity of mangroves to maintain position *in-situ* through vertical accretion, and mangroves were displaced landward *(9)*, with few exceptions *(10,11)*. During the early to mid Holocene, RSLR slowed in association with the final phase of

deglaciation of the Laurentide ice sheet *(12)*. The rate of RSLR varied across the globe due to glacio-isostatic adjustment, the response of the solid Earth and gravity field to ice mass redistribution during a glacial cycle (*13*). Far-field sites, those distal from regions of former ice sheet extent and incorporating most of the tropics, exhibit a decline in the rate of RSLR (*14*) from from 10,000 to 7,000 years ago (Phase 1 in Fig. 1A), followed by stable or falling sea level to near current position from ~6000 years ago to present (Phase 2 in Fig. 1A). In contrast, at intermediate-field sites closer to centres of glaciation (for example, the Gulf of Mexico and the Caribbean), sea level rose continuously throughout the Holocene due to isostatic response to melting of the Laurentide ice sheet. These coastlines have experienced a decelerating rate of RSLR from 10,000 years ago to the present (Fig. 1B and Figs. S5 and S6).

The spatially-variable deceleration of RSLR from 10,000 to 8,000 years ago across tropical and subtropical latitudes coincided with the initiation of vertically continuous, organic-rich mangrove sediments several metres thick, as rising seas flooded shallow continental shelves (Phase 1 in Fig. 1A,B) *(15)*. This deceleration provides an opportunity to explore whether: (i) the rate of mangrove vertical accretion responds to changes in RSLR; (ii) ice-sheet proximity (intermediate vs far field), geomorphic setting or tidal range constrain the capacity of mangroves to accrete in relation to RSLR; (iii) upper thresholds of mangrove vertical accretion can be detected; and (iv) mangrove development and vertical accretion correspond in timing to changes in the global atmospheric carbon budget.

We present empirical data from 122 reconstructions of the timing and rate of mangrove vertical accretion associated with Holocene RSLR in cores collected from 78 tropical and subtropical locations (Fig. 2, 14). We independently estimate rates of RSLR for each of the 78 locations

prior to and for the duration of mangrove vertical accretion from a glacio-isostatic adjustment model using an ensemble of different Earth parameters *(16)* (Fig. 3 and Figs. S5 and S6).

Slowing RSLR during the early to mid Holocene coincided with the initiation of extensive mangrove forests (Fig 1A, Phase 1; Fig. 3A,B). Our analysis suggests that sustained mangrove vertical accretion began across far-field regions (Africa, Asia, Australasia, South America) at ~10,000-8,000 years ago, and intermediate-field regions (Caribbean, Gulf of Mexico) at ~8,000-6,000 years ago (Fig. 3 and Figs. S1 and S2). Data were discriminated on the basis of ice-sheet proximity, geomorphic setting, and differentiated by tidal regime to explore differences in the timing of initiation and rates of vertical accretion (14). The intermediate- and far-field classifications, defined as a function of a location's proximity to areas of major ice sheet retreat during the last deglaciation, act as a surrogate variable for the temporal pattern of RSLR rates through the Holocene, which in turn influences the availability of accommodation space within which mangroves can accrete vertically. In a generalised linear model of several variables, only the proximity to former ice sheets proved to have a significant relationship with accretion rates (14).

We found a strong relationship ($p<0.001$) between rates of mangrove vertical accretion and RSLR rate across all sites (51% of the variation in the accretion rate can be explained by the RSLR variation; Fig. 3). Mangrove vertical accretion first initiated at ~9,800 years ago in the Ganges-Brahmaputra River Delta, as RSLR reduced from ~9 mm yr^{-1} to ~6 mm yr^{-1}, and continued for ~650 years at high rates until replaced by subtidal deposits as RSLR increased again to >7 mm yr^{-1} (14). Elsewhere in far-field locations, mangrove vertical accretion initiated as RSLR declined below ~7 mm yr^{-1} starting 8,800 years ago (Fig. 3). Rates of vertical accretion of >6 mm yr^{-1} were sustained for over 1,000 years in mangrove forests in Australia, Africa, South

America, Central America, and Asia (Fig. 2, Data S1), irrespective of geomorphic setting (Fig. S1).

Mangrove vertical accretion initiated in intermediate-field regions later than in far-field locations, first in Belize ~7,800 years ago as RSLR fell below ~5mm yr^{-1} and in other Caribbean and Gulf of Mexico sites between 7,500 and 6,000 years ago (Fig. 2 and Fig. 3 and Table S1). This later initiation, in comparison to far-field regions, may be related to the limited allochthonous sediment supply available in the carbonate (reef) settings, although in Belize rates of accretion of over 6 mm yr^{-1} were observed at two sites (Data S1), driven by strong authochthonous inputs.

We use a Bayesian framework to estimate the probability of initiation of mangrove accretion conditional upon rates of RSLR within the Holocene dataset (*14*). The empirical Holocene data (Data S1), which span a wide range of geomorphic settings and tidal regimes (Fig. S2), suggest that when RSLR rates exceed 6.1 mm yr^{-1} and 7.6 mm yr^{-1}, respectively, mangroves are very likely (>90% probability) and extremely likely (>95% probability) to be unable to initiate sustained accretion. We found lower RSLR thresholds for intermediate-field sites, and higher thresholds for far-field sites (Table 1).

Our database also reveals spatial variability in the duration of mangrove accretion (Figs. S1 and S2). In only three of 50 far-field locations was there indication of drowning of mangroves during a marine transgression (i.e., mangrove sediments overlain by tidal or subtidal deposits: Data S1). In most far-field locations (30 of 50), accretion and progrodation of the fluvial delta led to the replacement of mangrove by saltmarsh (characteristic of upper intertidal elevations), freshwater wetland, or terrestrial forest, often by the mid-Holocene when relative sea level stabilised (Data S1; Fig 1A Phase 2). For this reason, contemporary mangrove extent is highly contracted

compared to the early- and mid-Holocene mangrove development in many major river deltas such as the Ord River, Australia, the Red River, Vietnam, and the Mekong River, Vietnam and Cambodia *(15, 18-20)*. Mangrove accretion persisted significantly longer at intermediate-field locations (Fig. S2) because accommodation space was enhanced by glacio-isostatic adjustment.

The extensive development of mangrove environments under RSLR has exerted a significant influence on global carbon cycles over geologic timescales (*21*) including, we suggest, during the early to mid Holocene (Fig. 4). Carbon balance modelling based on stable carbon isotope signatures suggests that the 5 p.p.m.v reduction in atmospheric CO_2 in the early-Holocene was driven by increases in the uptake of carbon by the land biosphere on the order of 290 Pg C *(22,23)* prior to 7,000 years ago. The timing and volume of this uptake has been attributed to the northward expansion of boreal vegetation following ice-sheet retreat (~110 Pg C *(24)*), and organic soil development (180 Pg C *(23)*), of which circumarctic peatlands may have sequestered 20-60 Pg C based on the depth of peat formation at the time *(24)*. We conservatively estimate a somewhat larger contribution (~85 Pg C) from mangrove carbon sequestration and burial over the period 8,600 to 6,000 years ago (*14*). The extensive development of mangrove forests over this period largely replaced methanogenic environments (freshwater wetlands and floodplains (Data S1; *25*)) and corresponds to a declining rates of methane emission, particularly in the Southern Hemisphere (*26*). The $\delta^{13}CH_4$ signals in the Southern Hemisphere for this period show a 1.5‰ depletion consistent with a replacement of vegetation utilising the C_4 photosynthetic pathway (tropical grasslands and saltmarsh adapted to low atmospheric CO_2) with mangroves utilising the C_3 pathway *(26,27)*.

As RSLR increases in the 21st century, an increase in the rate of mangrove vertical accretion, coupled with landward expansion as sea level rises can be expected to drive increases in the rate

of carbon sequestration and preservation in mangroves environments, providing a negative feedback on radiative forcing, as suggested more broadly for coastal wetlands *(7)*. While our results demonstrate that accretion in mangroves increases in response to RSLR, we found it was very likely (>90% probability) that mangroves were unable to initiate sustained accretion when RSLR rates exceeded 6.1 mm yr^{-1} in any but the most sediment-laden settings. RSLR is projected to remain below 5 mm yr^{-1} under low emissions scenarios (RCP 2.6) throughout the 21st century *(1)*. However, RSLR is expected to exceed 5 mm yr^{-1} by 2030 and 7 mm yr^{-1} by 2050 under high emissions scenario RCP8.5 in low-latitude mangrove settings where rates of RSLR are expected to be higher than the global average (*1,2*).

Where a deficit commences between vertical accretion and RSLR, time to submergence will be a function of the position of the mangrove within the tidal frame. In settings of low tidal range mangroves are more likely to be situated at elevations close to the threshold of submergence from the outset. In settings of high tidal range, mangroves are more likely to be situated at elevations well above this threshold, and tolerate a deficit between the rates of accretion and RSLR for decades to centuries (*5*). Geomorphic setting will also influence vulnerability to submergence, as allochthonous sediment contributions in tide- and river-dominated estuaries may provide an elevation subsidy not available in environments receiving low sediment supply, such as coral reefs. In this context, sediment retention in catchments impacted by water resource development (i.e., trapped behind dams) and local sediment controls may decrease mangrove resilience to RSLR in river estuaries (*5*). The natural response of mangrove encroachment across flooded coastal lowlands is therefore the main determinant of future extent *(28)*, although this is already significantly impeded by coastal developments along many coastlines *(29)*. Our findings therefore emphasise the importance of (i) mitigating the magnitude of rapid RSLR, and (ii)

ensuring coastal adaptation measures allow for the expansion of mangrove across coastal lowlands.

References and Notes:

1. J.A. Church, et al. Sea Level Change. In: *Climate Change 2013: The Physical Science Basis. Contribution of Working Group I to the Fifth Assessment Report of the Intergovernmental Panel on Climate Change* [T.F. Stocker, D. Qin, G.-K. Plattner, M. Tignor, S.K. Allen, J. Boschung, et al. (eds.)]. Cambridge University Press, Cambridge, United Kingdom and New York, NY, USA. (2013).

2. R. E., Kopp, et al. Probabilistic 21st and 22nd century sea-level projections at a global network of tide-gauge sites. *Earth's future* ***2*****(8),** 383-406(2014).

3. M. L Kirwan, S. Temmerman, E.E. Skeehan, G.R. Guntenspergen, S. Fagherazzi, S. Overestimation of marsh vulnerability to sea level rise. *Nature Climate Change* ***6***, 253 (2016).

4. B. P. Horton, et al. Predicting marsh vulnerability to sea-level rise using Holocene relative sea-level data. *Nature communications*, ***9*****,** 2687 (2018).

5. C. E. Lovelock, et al. The vulnerability of Indo-Pacific mangrove forests to sea-level rise. *Nature*, ***526*****,** 559 (2015).

6. D. C Donato, J.B. Kauffman, D. Murdiyarso, S. Kurnianto, M. Stidham, M. Kanninen. Mangroves among the most carbon-rich forests in the tropics. *Nature geoscience*, ***4*****,** 293 (2011).

7. K. Rogers, et al. Wetland carbon storage controlled by millennial-scale variation in relative sea-level rise. *Nature*, ***567*****,** 91 (2019)

8. K. Lambeck, H. Rouby, A. Purcell, Y. Sun, M. Sambridge. Sea level and global ice volumes from the Last Glacial Maximum to the Holocene. *Proceedings of the National Academy of Sciences. U.S.A.* ***111*****,** 15296-15303 (2014).

9. C. D. Woodroffe. Mangrove response to sea level rise: palaeoecological insights from macrotidal systems in northern Australia. *Marine and Freshwater Research*, **69,** 917-932 (2018).

10. T. J. Hanebuth, H. K. Voris, Y. Yokoyama, Y. Saito, J. I. Okuno. Formation and fate of sedimentary depocentres on Southeast Asia's Sunda Shelf over the past sea-level cycle and biogeographic implications. *Earth-Science Reviews*, **104,** 92-110 (2011).

11. W. A. Nicholas, et al. Pockmark development in the Petrel Sub-basin, Timor Sea, Northern Australia: Seabed habitat mapping in support of CO2 storage assessments. *Continental Shelf Research*, **83,** 129-142 (2014).

12. N. S. Khan, et al. Holocene relative sea-level changes from near-, intermediate-, and far-field locations. *Current Climate Change Reports***, 1,** 247-262 (2015).

13. W.E. Farrell, J.A. Clark, J.A., On postglacial sea level. *Geophysical Journal International*, ***46***, 647-667 (1976).

14. Materials and methods are available as supplementary materials.

15. C. D Woodroffe, B. G. Thom, J. Chappell. Development of widespread mangrove swamps in mid-Holocene times in northern Australia. *Nature* **317,** 711. (1985).

16. S. Dendy, J. Austermann, J.R. Creveling, J.X. Mitrovica. Sensitivity of Last Interglacial sea-level high stands to ice sheet configuration during Marine Isotope Stage 6. *Quaternary Science Reviews* **171,** 234-244 (2017).

17. T. E. Törnqvist, N.P. Hijma. Links between early Holocene ice-sheet decay, sea-level rise and abrupt climate change. *Nature Geoscience* ***5*****,** 601 (2012).

18. B. G. Thom, L. D. Wright, J. M. Coleman. Mangrove ecology and deltaic-estuarine geomorphology: Cambridge Gulf-Ord River, Western Australia. *The Journal of Ecology*, 203-232. (1975).

19. S. A. Woodroffe, B. P. Horton. Holocene sea-level changes in the Indo-Pacific. *Journal of Asian Earth Sciences*, ***25*****,** 29-43 (2005).

20. S. Tanabe, K. Hori, Y. Saito, S. Haruyama, A. Kitamura. Song Hong (Red River) delta evolution related to millennium-scale Holocene sea-level changes. *Quaternary Science Reviews*, ***22*****,** 2345-2361. (2003).

21. D.S. Collins, et al. Tidal dynamics and mangrove carbon sequestration during the Oligo–Miocene in the South China Sea. *Nature Communications*, **8**, 15698. (2017).

22. A. Indermühle, et al. Holocene carbon-cycle dynamics based on CO_2 trapped in ice at Taylor Dome, Antarctica. *Nature*, ***398*****,**121 (1999).

23. J. Elsig, et al.. Stable isotope constraints on Holocene carbon cycle changes from an Antarctic ice core. *Nature*, ***461***, 507 (2009).

24. G. M. MacDonald, D. W. Beilman, K. V. Kremenetski, Y. Sheng, L. C. Smith, A. A. Velichko. Rapid early development of circumarctic peatlands and atmospheric CH4 and CO2 variations. *Science*, ***314*****,** 285-288 (2006).

25. H. J. Poffenbarger, B.A. Needelman, J.P. Megonigal. Salinity influence on methane emissions from tidal marshes. *Wetlands*, ***31*****,**831-842 (2011).

26. J. Beck, M. Bock, J. Schmitt, B. Seth, T. Blunier, H. Fischer (2018). Bipolar carbon and hydrogen isotope constraints on the Holocene methane budget. *Biogeosciences*, ***15*****,** 7155-7175.

27. T. Sowers. Atmospheric methane isotope records covering the Holocene period. *Quaternary Science Reviews* **29,** 213-221 (2010).

28. M., Schuerch et al. Future response of global coastal wetlands to sea-level rise. *Nature*, ***561*,** 231 (2018).

29. L. K., Phan, J. S. van Thiel de Vries, M. J. Stive. Coastal mangrove squeeze in the Mekong Delta. *Journal of Coastal Research*, ***31*,** 233-243. (2014).

30. S. E., Hamilton, D. Casey. Creation of a high spatio-temporal resolution global database of continuous mangrove forest cover for the 21st century (CGMFC-21). *Global Ecology and Biogeography*, ***25*,** 729-738. (2016).

31. K. L McKee, D.R. Cahoon, E.C. Feller. Caribbean mangroves adjust to rising sea level through biotic controls on change in soil elevation. *Global Ecology and Biogeography* ***16*,** 545-556 (2007).

32. C.D. Woodroffe. Mangrove sediments and Geomorphology. Chapter 2 in D. Alongi, A. Robertson, (eds.) *Tropical Mangrove Ecosystems*. American Geophysical Union, Coastal and Estuarine Studies, 7-41. (1992)

33. P.J. Reimer, et al. IntCal13 and Marine13 radiocarbon age calibration curves 0–50,000 years cal BP. *Radiocarbon*, ***55*,** 1869-1887. (2013).

34. M. A. Toscano, J.L. Gonzalez, K.R. Whelan. Calibrated density profiles of Caribbean mangrove peat sequences from computed tomography for assessment of peat preservation, compaction, and impacts on sea-level reconstructions. *Quaternary Research*, ***89*****,** 201-222 (2018).

35. D. F Argus, W.R. Peltier, R. Drummond, A.W. Moore. The Antarctica component of postglacial rebound model ICE-6G_C (VM5a) based on GPS positioning, exposure age dating of ice thicknesses, and relative sea level histories, *Geophysical Journal International*, **198,** 537–563 (2014).

36. W. R. Peltier, D.F. Argus, R. Drummond. Space geodesy constrains ice age terminal deglaciation: The global ICE-6G_C (VM5a) model, *Journal of Geophysical Research: Solid Earth*, **120**, 450– 487, (2015).

37. R. A Kendall, J.X. Mitrovica, G.A. Milne. On post-glacial sea level – II. Numerical formulation and comparative results on spherically symmetric models, *Geophysical Journal International*, **161**, 679–706, (2005)

38. Dziewonski, A. M., Anderson, D. L. Preliminary reference Earth model, *Physics of the Earth and Planetary Interiors*, **25**, 297-356, (1981)

39. E. Jones, et al. SciPy: Open Source Scientific Tools for Python, 2001 http://www.scipy.org/ [Online; accessed 2019-10-02].

40. F. Pedregosa et al.. Scikit-learn: Machine Learning in Python, *Journal of Machine Learning Research*, **12**, 2825-2830 (2011) (publisher link)

41. J. Goldberger, G. Hinton, S. Roweis, R. Salakhutdinov, "Neighbourhood Components Analysis". Advances in Neural Information", *Advances in Neural Information Processing Systems*, **17,** 513-520 (2005).

42. T. B Atwood, et al. Global patterns in mangrove soil carbon stocks and losses. *Nature Climate Change*, ***7***, 523. (2017).

43. C. M. Duarte, I.J. Losada, I.E. Hendriks, I. Mazarrasa, Marbà, N. The role of coastal plant communities for climate change mitigation and adaptation. *Nature Climate Change*, ***3*****,** 961. (2013).

44. K. Lamont, N. Saintilan, J.J. Kelleway, D. Mazumder, A. Zawadzki, A. Thirty-Year Repeat Measures of Mangrove Above-and Below-Ground Biomass Reveals Unexpectedly High Carbon Sequestration. *Ecosystems* 1-13 (2019)

45. M. Bock, J. Schmitt, J. Beck, B. Seth, J. Chappellaz, H. Fischer, H. Glacial/interglacial wetland, biomass burning, and geologic methane emissions constrained by dual stable isotopic

CH4 ice core records. *Proceedings of the National Academy of Sciences*, ***114,*** E5778-E5786. (2017).

46. R. Dommain, J. Couwenberg, P.H. Glaser, H. Joosten, I.N.N. Suryadiputra. Carbon storage and release in Indonesian peatlands since the last deglaciation. *Quaternary Science Reviews*, ***97***, 1-32 (2014).

47. N. Thomas, P. Bunting, R. Lucas, A. Rosenqvist, T. Fatoyinbo. Mapping mangrove extent and change: a globally applicable approach. *Remote Sensing* **10**, 1466 (2018)

48. A.P. Belperio. Negative evidence for a mid-Holocene high sea level along the coastal plain of the Great Barrier Reef province. *Marine Geology*, 32 (1979), pp. M1-M9

49. A.L. Bloom, 1975. In: D. Hopley (Editor), Research Report for Queensland. *Australian Quaternary Newsletter*, **5**: 22. (1979)

50. R.M. Carter, D. P. Johnson, K. G. Hooper Episodic post-glacial sea-level rise and the sedimentary evolution of a tropical continental embayment (Cleveland Bay, Great Barrier Reef shelf, Australia), *Australian Journal of Earth Sciences*, **40**, 229-255 (1993).

51. R. L. Clark, J.C. Guppy. A transition from mangrove forest to freshwater wetland in the monsoon tropics of Australia. *Journal of Biogeography* **15,** 665-684. (1988).

52. G. M Crowley, P. Anderson, A. P. Kershaw, J. Grindrod. Palynology of a Holocene marine transgressive sequence, lower Mulgrave River valley, north-east Queensland. *Australian Journal of Ecology*, ***15***, 231-240 (1990).

53. G. M. Crowley, M. K. Gagan. Holocene evolution of coastal wetlands in wet-tropical northeastern Australia. *The Holocene*, ***5***, 385-399. (1995).

54. T. R. Hashimoto, N. Saintilan, S.G. Haberle. Mid-Holocene development of mangrove communities featuring Rhizophoraceae and geomorphic change in the Richmond River Estuary, New South Wales, Australia. *Geographical Research*, ***44***, 63-76. (2006).

55. J. N. Jennings. Desert dunes and estuarine fill in the Fitzroy estuary (north-western Australia). *Catena*, ***2***, 215-262 (1975).

56. A.P. Spenceley. *The Geomorphological and Zonational Development of Mangrove Swamps in the Townsville Area, North Queensland*. PhD Thesis, James Cook University, Townsville (1980).

57. B. G. Thom, L. D. Wright, J. M. Coleman. Mangrove ecology and deltaic-estuarine geomorphology: Cambridge Gulf-Ord River, Western Australia. *The Journal of Ecology*, **63**, 203-232 (1975).

58. C. D. Woodroffe. Relative sea level in the South Alligator River region, north Australia, during the Holocene. *Search*, ***18***, 198-200 (1987).

59. C. D. Woodroffe, J. Chappell, B. G. Thom, E. Wallensky (1989). Depositional model of a macrotidal estuary and floodplain, South Alligator River, Northern Australia. *Sedimentology*, ***36***, 737-756.

60. J.C. Ellison. Pollen analysis of mangrove sediments as a sea-level indicator: assessment from Tongatapu, Tonga. *Palaeogeography, Palaeoclimatology, Palaeoecology*, ***74***, 327-341 (1989).

61. K. Fujimoto, T. Miyagi, T. Kikuchi, T. Kawana. Mangrove habitat formation and response to Holocene sea-level changes on Kosrae Island, Micronesia. *Mangroves and salt marshes*, **1**, 47-57 (1996).

62. K. Fujimoto, A. Imaya, R. Tabuchi, S. Kuramoto, H. Utsugi, T. Murofushi, Belowground carbon storage of Micronesian mangrove forests. *Ecological Research*, **14**, 409-413. (1999).

63. J.V. Ward. Palynology of Kosrae, Eastern Caroline Islands: Recoveries from pollen rain and Holocene deposits. *Review of Paleobotany and Palynology*, **55**, 247-271 (1988).

64. M. I., Bird, L. K. Fifield, T. S Teh, C. H. Chang, N. Shirlaw, K. Lambeck. An inflection in the rate of early mid-Holocene eustatic sea-level rise: A new sea-level curve from Singapore. *Estuarine, Coastal and Shelf Science*, ***71***, 523-536 (2007).

65. S. Das. Palaeo-palynology of late Quaternary peat deposit from Lower Bengal Basin, India: A palaoecological approach. *Quaternary international*, ***325***, 197-204 (2014).

66. J. Ellison. Holocene palynology and sea-level change in two estuaries in Southern Irian Jaya. *Palaeogeography, Palaeoclimatology, Palaeoecology*, ***220***, 291-309 (2005).

67. M. A. Geyh, H. Streif, H. R. Kudrass. Sea-level changes during the late Pleistocene and Holocene in the Strait of Malacca. *Nature*, ***278***, 441. (1979).

68. A.K. Hait, H. Behling. Holocene mangrove and coastal environmental changes in the western Ganga–Brahmaputra Delta, India. *Vegetation History and Archaeobotany*, ***18***, 159-169 (2009).

69. B. P. Horton, P. L. Gibbard, G. M. Mine, R. J. Morley, C. Purintavaragul, J.M. Stargardt. Holocene sea levels and palaeoenvironments, Malay-Thai Peninsula, southeast Asia. *The Holocene*, ***15***, 1199-1213 (2005).

70. M.S. Islam, M.J. Tooley. Coastal and sea-level changes during the Holocene in Bangladesh. *Quaternary International*, **55**, 61-75 (1999).

71. K. P. N. Kumaran, K. M., Nair, M. Shindikar, R. B. Limaye, D. Padmalal. Stratigraphical and palynological appraisal of the Late Quaternary mangrove deposits of the west coast of India. *Quaternary Research*, ***64***, 418-431 (2005).

72. Z. Li, et al. Mid-Holocene mangrove succession and its response to sea-level change in the upper Mekong River delta, Cambodia. *Quaternary Research*, ***78***, 386-399. (2012).

73. T. Rashid, S. Suzuki, H. Sato, M.H. Monsur, S.K., Saha. Relative sea-level changes during the Holocene in Bangladesh. *Journal of Asian Earth Sciences*, **64**, 136-150. (2013).

74. C.A Setyaningsih, S. Biagioni, A. Saad, K. Kashima, S. Sabiham, H. Behling. Response of Mangroves to Late Holocene Sea-Level Change: Palaeoecological Evidence from Sumatra, Indonesia. *Wetlands*, 1-16. (2019).

75. J. R. P. Somboon. Paleontological study of the recent marine sediments in the lower central plain, Thailand. *Journal of Southeast Asian Earth Sciences*, **2**, 201–210. (1988).

76. T. Tamura, Y. Saito, S. Sieng, B. Ben, M. Kong, I. Sim, S. Choup, F. Akiba. Initiation of the Mekong River delta at 8 ka: evidence from the sedimentary succession in the Cambodian lowland. *Quaternary Science Reviews*, **28**, 327–344. (2009).

77. S. Tanabe, K. Hori, Y. Saito, S. Haruyama, A. Kitamura. Song Hong (Red River) delta evolution related to millennium-scale Holocene sea-level changes. *Quaternary Science Reviews*, ***22***, 2345-2361 (2003).

78. N. Tran N., Q.T. Ngo. Development history of deposits in the Quaternary of Vietnam. In: T.V. Nguyen (ed) The Watehring Crust and Quaternary Sediments in Vietnam. Department of Geology and Minerals, Vietnam, Hanoi 177-198. (2000).

79. E. Yulianto, et al. Mangrove shoreline responses to Holocene environmental change, Makassar Strait, Indonesia. *Review of Palaeobotany and Palynology*, ***131***, 251-268. (2004).

80. J. F. Berger, V. Charpentier, R. Crassard, C. Martin, G. Davtian, J.A. López-Sáez. The dynamics of mangrove ecosystems, changes in sea level and the strategies of Neolithic settlements along the coast of Oman (6000–3000 cal. BC). *Journal of Archaeological Science*, ***40***, 3087-3104 (2013).

81. P. Punwong, K. Selby, R. Marchant. Holocene mangrove dynamics and relative sea-level changes along the Tanzanian coast, East Africa. *Estuarine, Coastal and Shelf Science*, ***212***, 105-117 (2018).

82. M. G. Tossou, A. Akoègninou, A. Ballouche, M.A. Sowunmi, K. Akpagana, K. The history of the mangrove vegetation in Bénin during the Holocene: a palynological study. *Journal of African Earth Sciences*, ***52***, 167-174 (2008).

83. S. A. Woodroffe, A. J. Long, P. Punwong, K. Selby, C.L. Bryant, R. Marchant. Radiocarbon dating of mangrove sediments to constrain Holocene relative sea-level change on Zanzibar in the southwest Indian Ocean. *The Holocene*, ***25***, 820-831 (2015).

84. H. Behling, M.C. Cohen, R.J. Lara. Studies on Holocene mangrove ecosystem dynamics of the Bragança Peninsula in north-eastern Pará, Brazil. *Palaeogeography, Palaeoclimatology, Palaeoecology*, **167**, 225-242 (2001).

85. T. Boski, F.H. Bezerra, L. de Fátima Pereira, A.M. Souza, R.P. Maia, F.P. Lima-Filho, F. P. Sea-level rise since 8.2 ka recorded in the sediments of the Potengi–Jundiai Estuary, NE Brasil. *Marine Geology*, ***365***, 1-13 (2015).

86. M.C.L Cohen, et al. Holocene palaeoenvironmental history of the Amazonian mangrove belt. *Quaternary Science Reviews*, **55**, 50-58 (2012).

87. M. C. L. Cohen, H. Behling, R.J. Lara, C.B. Smith, H.R.S. Matos, V. Vedel. Impact of sea-level and climatic changes on the Amazon coastal wetlands during the late Holocene. *Vegetation History and Archaeobotany*, **18**, 425. (2009).

88. M.C. Cohen, P.W. Souza Filho, R.J. Lara, H. Behling, R.J. Angulo. A model of Holocene mangrove development and relative sea-level changes on the Bragança Peninsula (northern Brazil). *Wetlands Ecology and Management*, **13**, 433-443 (2005).

89. N. A. Fontes, et al. The impacts of the middle Holocene high sea-level stand and climatic changes on mangroves of the Jucuruçu River, southern Bahia–northeastern Brazil. *Radiocarbon*, ***59***, 215-230 (2017).

90. M. C. França, et al. The last mangroves of Marajó Island—Eastern Amazon: impact of climate and/or relative sea-level changes. *Review of Palaeobotany and Palynology*, ***187***, 50-65 (2012).

91. M. C. França, et al. Mangrove vegetation changes on Holocene terraces of the Doce River, southeastern Brazil. *Catena*, ***110***, 59-69 (2013).

92. J. T. F. Guimarães, M. C. L Cohen, L. C. R. Pessenda, M. C. França, C. B. Smith, A. C. R Nogueira. Mid-and late-Holocene sedimentary process and palaeovegetation changes near the mouth of the Amazon River. *The Holocene*, ***22***, 359-370 (2012).

93. W. Roeleveld, A.J. van Loon. The Holocene development of the Young Coastal Plain of Suriname. *Geol. En Mijnb*. **58**, 21–28 (1979).

94. V. Rull, T. Vegas-Vilarrubia, N.E. de Pernia. Palynological record of an early-mid Holocene mangrove in eastern Venezuela. Implications for sea-level rise and disturbance history. *Journal of Coastal Research*, 496-504 (1999).

95. L. E Urrego, A.Correa-Metrio, C. González, A.R. Castaño, Y. Yokoyama. Contrasting responses of two Caribbean mangroves to sea-level rise in the Guajira Peninsula (Colombian Caribbean). *Palaeogeography, Palaeoclimatology, Palaeoecology*, ***370***, 92-102 (2013).

96. V. Vedel, H. Behling, M. Cohen, R. Lara. Holocene mangrove dynamics and sea-level changes in northern Brazil, inferences from the Taperebal core in northeastern Pará State. *Vegetation History and Archaeobotany*, ***15***, 115-123. (2006).

97. T. A. Bianchette, T. A McCloskey, K.B. Liu. A 7000-year history of coastal environmental changes from Mexico's Pacific Coast: A multi-proxy record from Laguna Mitla, Guerrero. *The Holocene*, ***27***, 1214-1226. (2017).

98. C. Cordero-Oviedo, et al. Holocene establishment of mangrove forests in the western coast of the Gulf of Mexico. *Catena*, **180**, 212-223 (2019).

99. G. Digerfeldt, M.D. Hendry. An 8000 year Holocene sea-level record from Jamaica: implications for interpretation of Caribbean reef and coastal history. *Coral Reefs*, **5**, 165-169 (1987).

100. J. C. Ellison. Mangrove retreat with rising sea-level, Bermuda. *Estuarine, Coastal and Shelf Science*, ***37***, 75-87 (1993).

101. P. Ezcurra, E. Ezcurra, P.P. Garcillán, M.T. Costa, M. T., O. Aburto-Oropeza. Coastal landforms and accumulation of mangrove peat increase carbon sequestration and storage. *Proceedings of the National Academy of Sciences*, ***113***, 4404-4409. (2016).

102. C. Feller, M. Fournier, D. Imbert, C. Caratini, L. Martin. Datations 14C et palynologie d'un sédiment tourbeux continu (0-7 m) dans la Mangrove de Guadeloupe (FWI). Résultats préliminaires. In M.P. Prost: Evolution des littoraux de Guyane et de la zone Caraïbe méridionale pendant le Quaternaire, Symposium PICG (Vol. 274, pp. 193-202). (1992).

103. J. C. Joo-Chang, G.A. Islebe, N. Torrescano-Valle. Mangrove history during middle-and late-Holocene in Pacific south-eastern Mexico. *The Holocene*, *25*(4), 651-662. (2015).

104. N.S. Khan. *Environmental and sea-level reconstruction in temperate, subtropical, and tropical coastal wetlands using bulk stable carbon isotope geochemistry and microfossils* (Ph.D. Dissertation). University of Pennsylvania, Philadelphia. (2014).

105. I.G. Macintyre, M.M. Littler, D.S. Littler. Holocene history of Tobacco Range, Belize, Central America. Atoll Research Bulletin **430,** 1-18 (1995).

106. I.G. Macintyre, M.A. Toscano, R.G. Lighty, G.B. Bond. Holocene history of the mangrove islands of Twin Cays, Belize, Central America. Atoll Research Bulletin **510,** 1-16 (2004).

107. S.J. Mazzullo, C.S. Teal, W.D. Bischoff, K. Dimmick-Wells, B.W. Wilhite. Sedimentary architecture and genesis of Holocene shallow-water mud-mounds, northern Belize. *Sedimentology* **50**, 743–770 (2003).

108. N. M. Monacci, U. Meier-Grünhagen, B.P. Finney, H. Behling, M.J. Wooller. Mangrove ecosystem changes during the Holocene at Spanish lookout Cay, Belize. *Palaeogeography, Palaeoclimatology, Palaeoecology*, ***280***, 37-46. (2009).

109. N. M. Monacci, U. Meier-Grünhagen, B.P. Finney, H. Behling, M.J. Wooller. Paleoecology of mangroves along the Sibun River, Belize. *Quaternary Research*, ***76***, 220-228. (2011).

110. D. W. Scholl. Recent sedimentary record in mangrove swamps and rise in sea level over the southwestern coast of Florida: Part 2. *Marine Geology*, ***2***, 343-364. (1964).

111. R.J. Shlemon, J.L. Capacete. Application of holocene geological data for siting coastal nuclear power plants: An example from Puerto Rico. *Bulletin of the International Association of Engineering Geology* **13**, 107–111 (1976).

112. E.K. Ramcharan, J.H. McAndrews. Holocene development of coastal wetland at Maracas bay, Trinidad, West Indies. *Journal of Coastal Research*, 581-586 (2006).

113. E. K. Ramcharan. Mid-to-late Holocene sea level influence on coastal wetland development in Trinidad. *Quaternary International*, ***120***, 145-151 (2004).

114. E.K. Ramcharan. Late Holocene ecological development of the Graeme Hall swamp, Barbados, West Indies. *Caribbean Journal of Science,* **41**, 14 (2005).

115. D.M. Robbin. A new Holocene sea-level curve for the upper Florida Keys and Florida reef tract. In: P.J. Gleason (ed) *Environments of south Florida, present and past*. Miami Geological Society, 437–458 (1984).

116. D.P. Schmidt. *A palynological and stratigraphic analysis of mangrove sediments at Punta Galeta, Panamá*. University of California, Berkeley (2008).

117. N. Torrescano, G.A. Islebe. Tropical forest and mangrove history from southeastern Mexico: a 5000 yr pollen record and implications for sea level rise. *Veg. Hist. Archaeobotany* **15**, 191–195 (2006).

118. C. D. Woodroffe. Mangrove swamp stratigraphy and Holocene transgression, Grand Cayman Island, West Indies. *Marine Geology*, ***41***, 271-294 (1981).

119. M. J. Wooller, H. Behling, B.J. Smallwood, M. Fogel. Mangrove ecosystem dynamics and elemental cycling at Twin Cays, Belize, during the Holocene. *Journal of Quaternary Science*, ***19***, 703-711(2004).

120. M.J. Wooller, R. Morgan, S. Fowell, H. Behling, M. Fogel. A multiproxy peat record of Holocene mangrove palaeoecology from Twin Cays, Belize. *The Holocene*, **17**, (2007).

121. Q. Yao, K.B. Liu, W.J. Platt, V.H. Rivera-Monroy. Palynological reconstruction of environmental changes in coastal wetlands of the Florida Everglades since the mid-Holocene. *Quaternary Research*, **83**, 449-458 (2015).

122. Q. Yao, K.B. Liu. Dynamics of marsh-mangrove ecotone since the mid-Holocene: A palynological study of mangrove encroachment and sea level rise in the Shark River Estuary, Florida. *PloS one*, **12**, p.e0173670 (2017).

123. P.S. Filho, M.C.L. Cohen, R.J. Lara, G.C. Lessa, B. Koch, H. Behling. Holocene coastal evolution and facies model of the Bragança macrotidal flat on the Amazon Mangrove Coast, Northern Brazil. *Journal of Coastal Research*, 306-310. (2006).

124. M. J.Wooller, H. Behling, J. L. Guerrero, N. Jantz, M. E Zweigert. Late Holocene hydrologic and vegetation changes at Turneffe Atoll, Belize, compared with records from mainland Central America and Mexico. *Palaios*, ***24***, 650-656. (2009).

125. J.J. Kelleway, et al. Geochemical analyses reveal the importance of environmental history for blue carbon sequestration. *Journal of Geophysical Research: Biogeosciences,* **122**, 1789-1805. (2017).

126. G.D. Egbert, S.Y, Erofeeva. Efficient inverse modeling of barotropic ocean tides. *Journal of Atmospheric and Oceanic Technology*. **19**, 183-204. (2002).

5

10

15

20

25

30

Acknowledgments: We thank Jerry Mitrovica of Harvard University for providing the GIA model. Timothy A. Shaw of Nanyang Technology University assisted with the preparation of figures. Figure 1 utilised the image library of the Integration and Application Network, University of Maryland Centre for Environmental Science (ian.umces.edu/imagelibrary/). **Funding:** NS was supported by an Outside Studies Program grant from Macquarie University and AINSE. BPH are supported by the Singapore Ministry of Education Academic Research Fund MOE2018-T2-1-030, the National Research Foundation Singapore, and the Singapore Ministry of Education, under the Research Centers of Excellence initiative. This article is a contribution to PALSEA2 (Palaeo-Constraints on Sea-Level Rise) and International Geoscience Program (IGCP) Project 639, "Sea-Level Changes from Minutes to Millennia". This work is Earth Observatory of Singapore contribution 294. KR received funding from the Australian Research Council (FT130100532). **Author contributions:** NS conceived the study. NS, NSK and BPH assembled the contributing mangrove sediment data. EA extracted RSLR estimates from GIA models. NS, EA and JK conducted data analyses. NS, NSK, EA, and KR prepared figures. All authors contributed to the writing of the manuscript. **Competing interests:** Authors declare no competing interests. **Data and materials availability:** All data is available in the main text or the supplementary materials.

Supplementary Materials:

Materials and Methods

Figures S1-S6

Tables S1-S2

External Database S1

References (*30-126*)

FIGURES

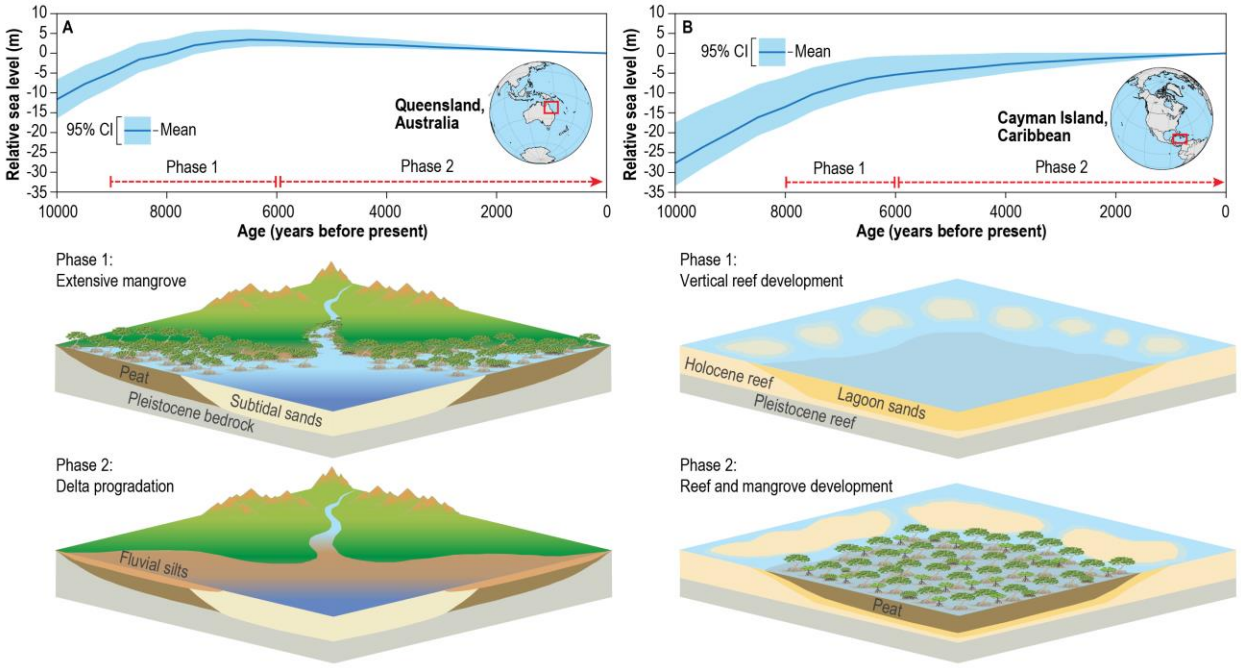

Fig. 1: **Holocene RSLR and associated mangrove development in (A) far-field estuarine and (B) intermediate-field calcareous settings**. As the rate of RSLR decelerated, development of organic-rich mangrove sediments was initiated, facilitating maintenance of vertical position with respect to sea level, forming extensive mangrove forests. When RSLR stabilises, ongoing sedimentation infills estuaries, building deltas and replacing mangrove with freshwater wetlands, terrestrial forest or saltpan, depending on climatic setting.

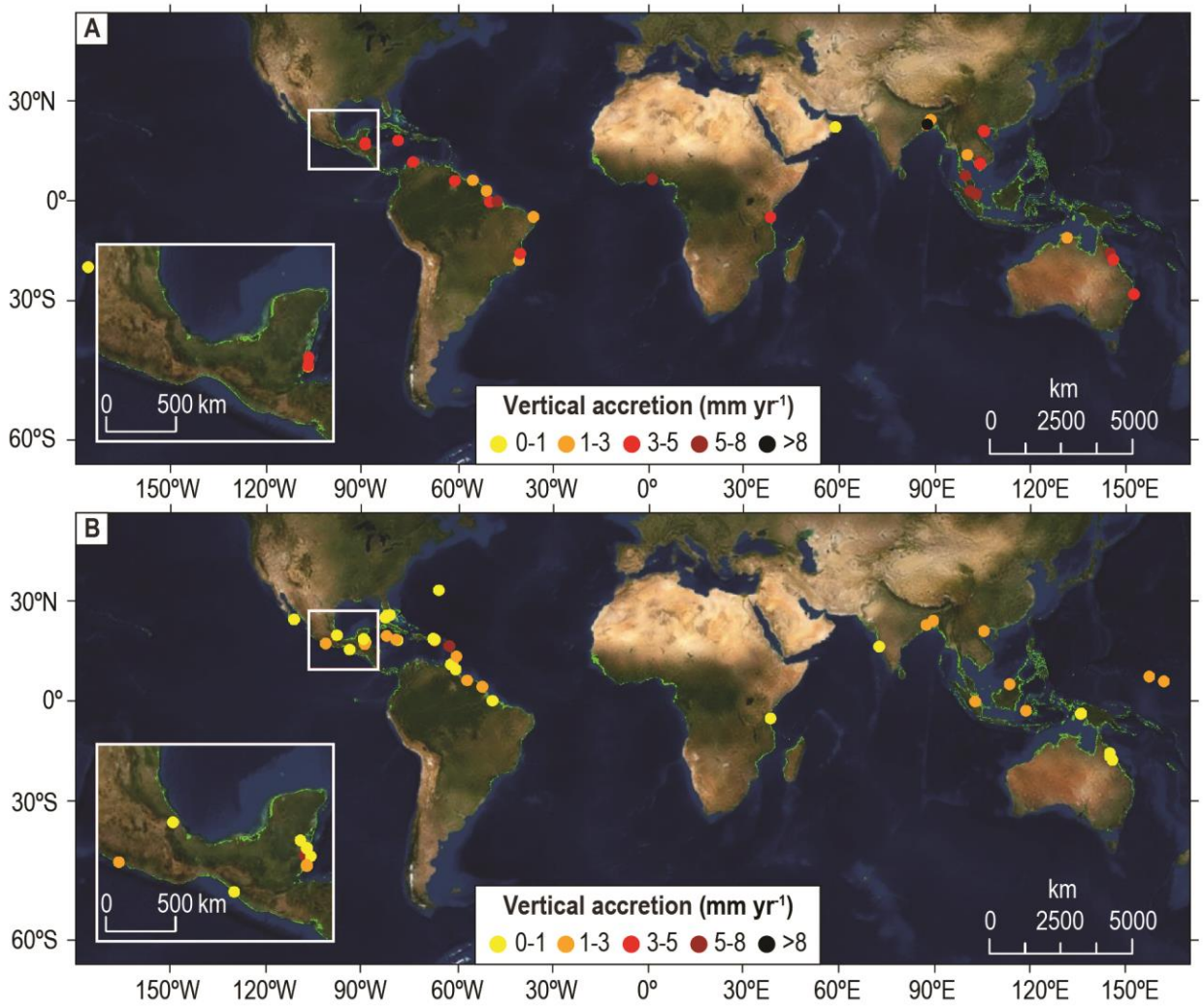

Fig. 2: **Sampling locations and corresponding rates of mangrove vertical accretion**. Mangrove sedimentary units initiating between between 10,000 and 6,500 years ago (top panel) and mangrove sedimentary units initiating following 6,500 years ago (lower panel). Contemporary mangrove shorelines are indicated in bright green representing mangrove distribution in 2012 *(30)*.

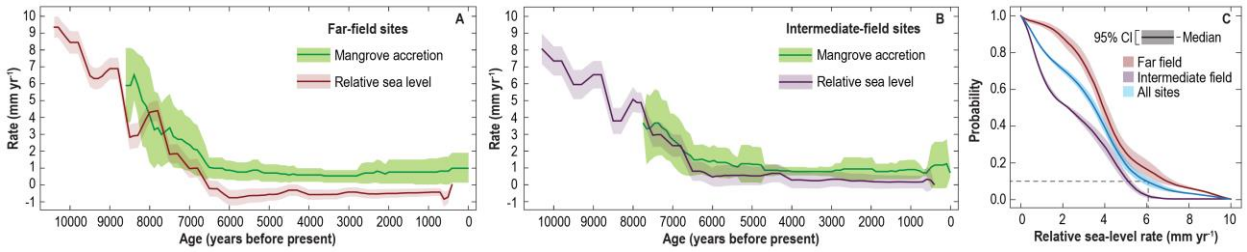

Fig. 3: **Rates of mangrove vertical accretion and RSLR.** Accretion rates are derived from the depth of mangrove organic sediment between calibrated ^{14}C dates in individual cores, and rates of RSLR (median and 95% credible interval (CI)) were derived from the GIA model ensemble for the same sites for (A) far-field and (B) intermediate-field locations. (C) The probability of initiation of sustained mangrove accretion at or above associated rates of RSLR across all sites. The dotted line shows the RSLR rate at which there is a 10% probability that mangroves can initiate accretion, and/or conversely that there is a 90% probability they are unable to initiate accretion.

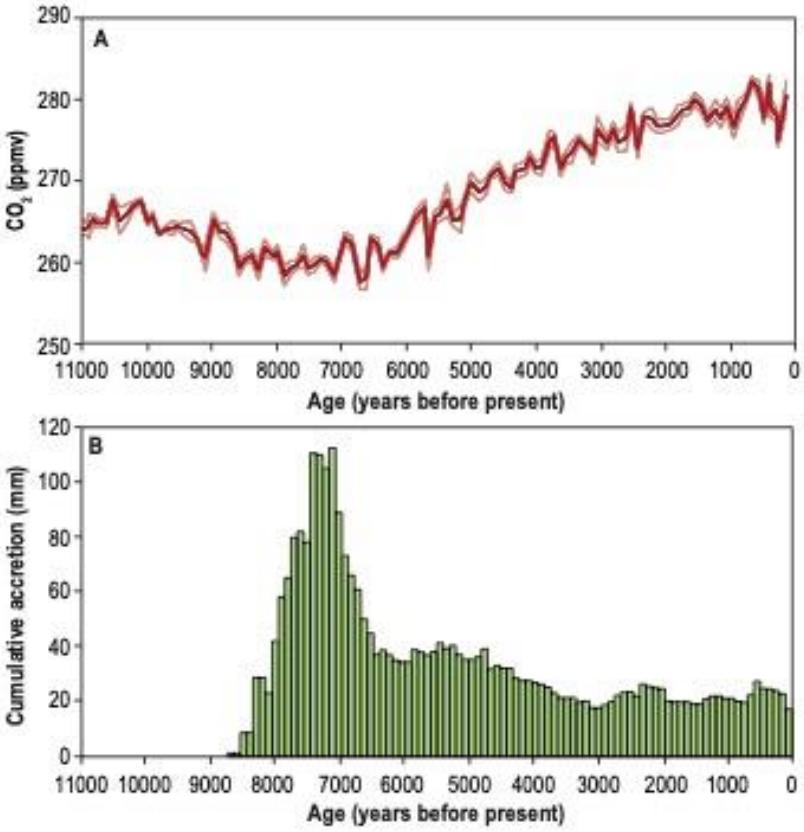

Fig. 4. **Timing of mangrove vertical accretion in relation to greenhouse gas concentrations.** (A) Atmospheric CO_2 concentrations (from Antarctic ice-cores *(23)*) and (B) mangrove organic soil formation (the sum of all observations spanning each century weighted by the vertical accretion rate of each observation (*14*)). Light coloured curves in A and represent ± 1 standard error for CO_2 (b), as presented in the original datasets.

Table 1: **Probability mangroves are unable to initiate sustained vertical accretion at rates of RSLR** (*14*). RSLR rates at all sites (global) and intermediate- and far-field sites at which it is very likely (>90% probability) and extremely likely (>95% probability) for mangroves to be unable to initiate sustained accretion, and the associated 95% uncertainty interval (UI). For example, at all sites, there is a 94.3 – 95.4% probability (95% UI) that mangroves are unable to initiate at rates that exceed 7.6 mm yr^{-1}.

	RSLR rates (mm yr^{-1}) above which accretion did not initiate (Very Likely: 90% median probability)	(uncertainty interval)	RSLR rates (mm yr^{-1}) above which accretion did not initiate (Extremely Likely:95% median probability)	(uncertainty interval)
Global	6.1	(88.1 – 92.8)	7.6	(94.3 – 95.4)
Intermediate Field (Gulf of Mexico, Caribbean)	5.2	(88.1 – 92.8)	5.7	(93.7 – 96.9)
Far field	7.1	(87.3 – 91.6)	8.8	(94.4 – 95.8)

Science
AAAS

Supplementary Materials for

Thresholds of mangrove survival under sea-level rise

N. Saintilan*, N.S. Khan, E. Ashe, J.J. Kelleway, K. Rogers, C.D. Woodroffe, B.P. Horton
Correspondence to: neil.saintilan@mq.edu.au

Other Supplementary Materials for this manuscript include the following:

Data S1

Materials and Methods

Accretion Rates

We searched for all published studies reporting on Holocene transgressive organic-rich mangrove sediments using online search engines (Google Scholar, Web of Science) and our own databases. From 190 studies we selected cores conforming to the following criteria: (a) material consisted of mangrove organic muds or peats of at least two metres in depth (i.e. greater than the rooting depth of mangrove and therefore implying *in-situ* vertical accretion) (b) mangrove presence was confirmed by either pollen analysis or the identification of mangrove root morphology and (c) radiocarbon dates were available for at least two positions in individual cores separated by a depth of at least 1 metre (the maximum rooting depth) and at least ~300 years. Of the 73 studies conforming to these requirements, we extracted information from 122 core sections (from 90 cores) spanning 78 locations, with an average vertical interval between ^{14}C dates of 2.5 m (± 1.2 m), and average time interval between ^{14}C dates of 1931 cal years (± 1849) (Data S1; *31; 46-121*).

We noted the location, and recorded latitude and longitude of each core. We interpreted its geomorphic setting using the categories (after *32*) of tide-dominated estuarine (macro to meso-tidal with the funnel mouth characteristic of tide dominance), barrier estuarine (in which mangrove development occurs behind protective sand barriers on wave dominated coastlines), large river delta (in which fluvial discharge and sedimentation are the dominant processes), carbonate (i.e. coral reef including both oceanic island and barrier reef settings), and coastal embayment (i.e. sheltered open coast or open embayment with minimal fluvial input). We also estimated local tidal range for each site using the OSU TPXO9 global tidal model (*126*) and classified sites as micro- (great diurnal range [GT] < 2 m), meso- (GT between 2 to 4 m) and

macrotidal (GT > 4 m). We interpreted the environment pre-dating and post-dating mangrove formation on the basis of pollen and stratigraphic descriptions to infer the nature (i.e., transgressive, regressive) of contacts below and above mangrove sequence where possible. The dominant mangrove species were noted.

We extracted radiocarbon dates and uncertainties representing (i) the earliest date for mangrove initiation at the site; (ii) the latest date for mangrove survival at the site; (iii) the date corresponding to the beginning of the single core sequence from which an accretion rate was estimated; and (iv) the end date of the single core sequence from which an accretion rate was estimated. We calibrated all radiometric dates to sidereal years using IntCal13 (*33*) and SHCal13 within Calib 7.10 (http://calib.org/calib/calib.html). We reported 2σ age ranges (Data S1).

We calculated rates of accretion as the depth of mangrove organic sediment between the 2σ midpoints of calibrated radiocarbon dates divided by the time interval between dates, a technique previously applied to estimate mangrove vertical accretion in Belize *(31)*. Accretion rates are averaged over the time period between dates, and do not reflect variability in accretion rate over shorter time periods. Given the rapid deceleration of eustatics sea level rise over the early Holocene, these rates are likely to be conservative. Mangrove root material is largely refractory *(31)* under conditions of rising sea level and the high water content and hydraulic conductivity of mangrove peats limit dewatering and compaction *(34)*.

The sample distribution is biased to land-based samples and, in general, the upper 10-15 metres of Holocene sediment. The deepest core (ID27: Ganges-Brahmaputra River) in our sample

extended to 50 metres and included a transgressive mangrove soil in the lowest 9 metres, the oldest mangrove sample in our dataset and that with the highest estimated accretion rate. Fifteen cores did not extend to the lower depth of the mangrove unit. Similarly, the lack of off-shore sampling, may exclude locations that maintained high rates of vertical accretion over appreciable periods of time, and bias our sampling towards habitats that survived RSLR. Our sampling of mangrove accretion in the very early Holocene (pre-9000BP) is thereby limited. Mangrove cumulative accretion (Fig. 4) is the sum of all observations of mangrove vertical accretion occurring in each century, multiplied by the accretion rate for each observation. Mangrove root material is largely refractory *(31)* under conditions of rising sea level and the high water content and hydraulic conductivity of mangrove peats limit dewatering and compaction *(34)*.

Glacial Isostatic Adjustment Modelling

Rates of local and regional RSL change during the Holocene are primarily the result of glacio-isostatic adjustment (GIA), the loss of ice burden and subsequent deformational, rotational and gravitational effects on the solid Earth that influences both both eustatic and relative sea level. We use a revised model of glacio-isostatic adjustment *(16)*, which adopts the ICE-6G global ice reconstruction from the Last Glacial Maximum (LGM) to the present day *(35,36)*. The sea-level calculations are based on a gravitationally self-consistent eustatic and relative sea level. We use a revised model of glacio-isostatic adjustment *(16)*, which adopts the ICE-6G global ice reconstruction from the Last Glacial theory that incorporates time-varying shorelines and the feedback of load-induced perturbations to Earth's rotation into sea level *(37)*. The model assumes a spherically symmetric, self-gravitating, Maxwell viscoelastic Earth model. The elastic and density components of the model are given by the seismic model PREM *(38)* and the

viscosity structure is characterized by three parameters: an infinite viscosity (elastic) lithosphere of prescribed thickness, *LT*, and upper and lower mantle viscosities denoted by V_{UM} and V_{LM}, respectively.

We used 300 combinations of these Earth rheological parameters in the glacio-isostatic adjustment model to predict RSL heights at a 512 x 260 global grid at 500-year periods. The ensemble of 300 combinations of parameters included *LT* from 24 – 140 km, V_{UM} from 0.3 – 2 x 10^{21}Pas, and V_{LM} from 3 – 100 x 10^{21}Pas, where each combination is assumed to be equally likely. These ensemble predictions provided uncertainty in RSLR rates of change for each site in this study.

Statistical analysis

We previously demonstrated that spatial and temporal variations in RSLR over the mid- to late-Holocene act as a global control on persistence of organic matter in coastal wetlands substrates *(7)*. We hypothesise therefore that the duration of mangrove growth (as evidenced by continuous mangrove substrate within a given core) will vary between intermediate-field and far-field locations, with longer persistence in intermediate-field zones relative to far-field locations where RSLR stabilised several millennia earlier (NB Mangroves do not grow in near-field locations).

Generalised linear models were used to test the correlations between several variables. We tested whether the non-normal variable mangrove duration (count of years mangrove persisted *in situ*) varied between intermediate and far-field locations assuming a Poisson distribution and using a log link function. Mangrove initiation date was included as a covariate in pairwise comparisons

and was based on estimated marginal means subject to Bonferroni adjustment. Additionally, we tested whether the mangrove accretion rates varied between intermediate and far-field locations, geomorphic settings, and tidal ranges (Table S1) assuming a Gaussian distribution and using an identity link function. We also tested the relationship between mangrove accretion rate and RSLR rate from the mean time during accretion assuming a Gaussian distribution and using an identity link function (Fig S5; Table S1). A significance level of $P<0.05$ was employed for all models.

The statistical analysis of RSLR is based on the glacio-isostatic adjustment modelling described above. We linearly interpolate relative sea level heights between the spatial and temporal predictions at sites and dates from the mangrove data using scipy's interpolate package *(39)*. We calculate RSLR rates using a linear transformation and approximate the rate distribution using kernel density estimation with sklearn.neighbors.kde *(40,41)* enabling the estimation of a cumulative distribution function (cdf) for each set of rates. We split all sites of mangrove accretion into two categories (intermediate- and far-field sites), based on their proximity to the former Laurentide Ice Sheet. Using 300-year average rates estimated every 100 years, we estimate RSLR during accretion times for far-field and intermediate-field sites by averaging RSLR at all sites where mangrove is within an accretion period (between the 95th percentile of the beginning of accretion through the 5th percentile of termination) (Fig. 3).

To estimate the probability of initiation of mangrove accretion conditional upon rates of RSLR within this dataset, we use a Bayesian framework to invert the probability of RSLR, given initiation of mangrove accretion $p(y|x)$, where:

$$p(x|y) \propto p(y|x)p(x)$$

The posterior probability of initiation given RSLR, $p(x|y)$, is therefore proportional to $p(y|x)$. We model $p(x|y)$ using kernel density estimation (KDE):

$$p(y|x) = \begin{cases} \frac{1}{nh}\sum_{i=1}^{n} K\left(\frac{y-y_i}{h}\right), & \text{when } x = 1 \\ 0, & \text{when } x = 0 \end{cases}$$

where *K* is a non-negative normal kernel, *h* is a smoothing parameter (or bandwidth), *n* is the number of RSLR estimates used in the KDE during which mangrove is initiating. The parameter *h* is optimized through unsupervised nearest neighbors learning *(40,41)*. We use an uninformative prior distribution of initiation, $p(x)$, where *p(1) = p(0) = 0.5*. We use Monte Carlo methods to generate 1000 independent samples of RSLR at initiation, assuming a uniform distribution within the 95% CI of radiocarbon dates. The distribution of RSLR at initiation with uncertainties is the combination of all KDEs of the probability density functions for each sample. We invert the cumulative distribution functions of initiation rates to find the probability of mangrove initiation given RSLR with uncertainty. For example, the probability that mangroves initiated at RSLR rates of exceeding 6.1 mm yr^{-1} and 7.6 mm yr^{-1}, respectively, at the time of initiation is ~ 10% (95% Uncertainty Interval (UI): 7.9 – 12.2 %) and ~ 5% (UI: 4.6% – 5.7%). Assuming an uninformative prior distribution on initiation translates RSLR rates exceeding 6.1 mm yr^{-1} and 7.6 mm yr^{-1}, respectively, suggesting that mangroves are very likely (>90% probability; 95 % Uncertainty Interval (UI): 87.8 – 92.1%) and extremely likely (>95% probability; 95% UI: 94.3 – 95.4%) to be unable to initiate sustained accretion. The probabilities of initiation of sustained mangrove accretion at a given RSLR rate are summarized in Fig. 3c and Table S1. All RSLR analyses based on glacia-isostatic modelling were implemented in the software package Python.

Carbon sequestration and GHG Emissions Factors

Most of the papers dealing with early to mid Holocene mangrove development in far field locations comment on a substantially greater mangrove aerial extent at this time compared to current distribution. These include major river deltas of Southeast Asia: the Song (20); the Mekong (72,76); the Malay-Thai Peninsula (69); west coast India (71); the macrotidal estuaries of northern Australia, reviewed in (15), and including the Ord (57), the Fitzroy (55), the South Alligator (59); mesotidal estuaries on the Australian east coast (52-54); the Ivory coast, Africa (82), Bragança Peninsula, Brazil (84), and the coastal plain of Suriname (93) and Venezuela (94). Mangrove extent contracted with infilling, to a degree difficult to constrain with the limited spread of point measures from the early Holocene. For this reason, and our limited understanding of Holocene distribution outside of these major deltaic systems, we have refrained from estimating early Holocene global mangrove extent. For our estimates of carbon sequestration from this time, we use the conservative value of current mangrove extent.

Current estimates of the global carbon store in the upper metre of the world's mangroves vary due primarily to differences in the calculation of mangrove area, from 2.6 Pg C *(42)* to 9.4-10.4 Pg C *(43)*, with an additional 1.8 Pg C in above-ground biomass *(43)*. These estimates are based on soil organic carbon stores of 283 ± 193 Mg C ha−1 (±s.d.) (*42*) and 255 Mg C ha−1 (*43*), the differing stores being primarily due to different area estimates (*42*).

Following the initiation of the phase of extensive mangrove development as RSLR fell below 7mm yr^{-1} ~8800 years ago and extending to 6000 years ago, we estimated vertical accretion

using the average across all sites (Data S1). On these estimates, mangroves in the early-Holocene would have accreted ~8 m and sequestered ~85 Pg C between 8200 and 6000, on the conservative assumptions that (i) mangrove area in this period was not greater than the contemporary estimate of (*47*) and (ii) that the efficiency of carbon capture under rapidly rising sea-level was not less than at present. We also assume that mangrove soil organic carbon is predominantly autochthonous, as suggested by studies using direct measurement and/or stable isotope approaches (*44*).

We do not anticipate appreciable loss of carbon with depth in most of these settings during the transgressive phase. Carbon is efficiently retained in soils subject to rapid sea-level rise (*7*). This is because the depth of oxygen penetration in saturated soils is 1-10mm (*21*). A portion of surficial organic carbon is therefore buried within a year, but most new organic carbon is introduced by roots at greater depths (*44*). Studies in the Caribbean (*31*) and Australia (125) shows excellent preservation of old root material.

There are several lines of evidence to suggest that tropical mangroves may have played a role in forcing changes to atmospheric methane concentrations during the Holocene. The deuterium stable isotope ratio ($\delta D\text{-}E_s$) of ice-core CH_4 during the period suggests shifts in CH_4 emissions to be dominated by tropical wetlands rather than geological emissions *(45)*, consistent with local sea-level stabilisation forcing increases in the extent of freshwater wetland in Indonesia *(46)* and other large tropical systems *(45)*. This corresponds to a period in which tropical mangroves were replaced by methanogenic wetlands (freshwater sedges) and rainforest following the stabilisation of sea levels in the Southern Hemisphere and the Indo-Pacific (Data S1).

SUPPLIMENTARY FIGURES

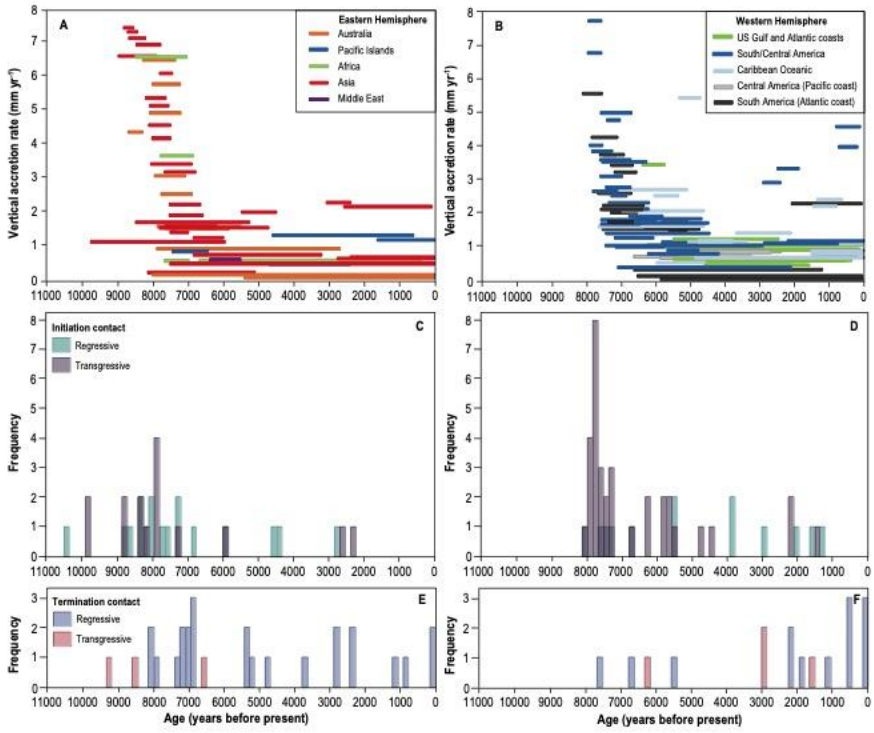

Fig S1. Rates of mangrove vertical accretion and the nature of initiation and termination contacts (i.e., transgressive vs. regressive) above and below mangrove sequences throughout the Holocene.

Rates of mangrove vertical accretion are shown for the Eastern (A) and Western (B) hemisphere between calibrated ^{14}C dates in individual cores (Data S1). Horizontal bars represent the individual mangrove stratigraphic units between ^{14}C-dated organic material. Rate of vertical accretion is calculated as the vertical difference divided by the age difference, as explained in Materials and Methods. Nature of initiation (C, D) and termination (E, F) stratigraphic contacts below and above mangrove sequences through time.

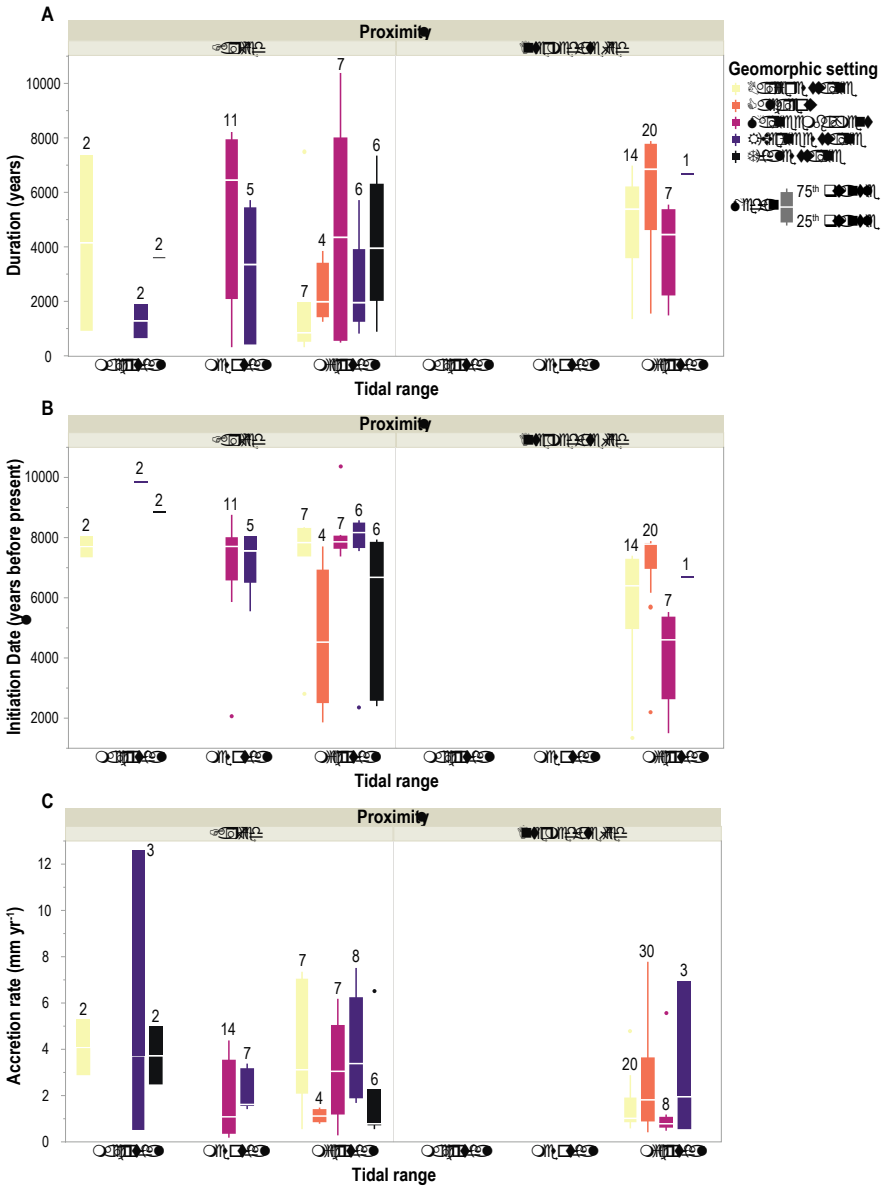

Fig S2. Variability of mangrove duration, initiation date, and vertical accretion rate associated with proximity to former ice sheets, geomorphic setting, and tidal regime. Box and whisker plots show the duration of mangrove accretion (A), the initiation date of sustained mangrove accretion (B), and the mangrove vertical accretion rate (C) by proximity to former ice sheets (far-, intermediate-field), tidal range (macro-, meso-, and microtidal), and geomorphic setting (barrier estuarine, calcareous, marine embayment, riverine estuarine, tidal estuarine). Numbers above boxes indicate sample size. Whiskers represent 1.5x the interquartile range.

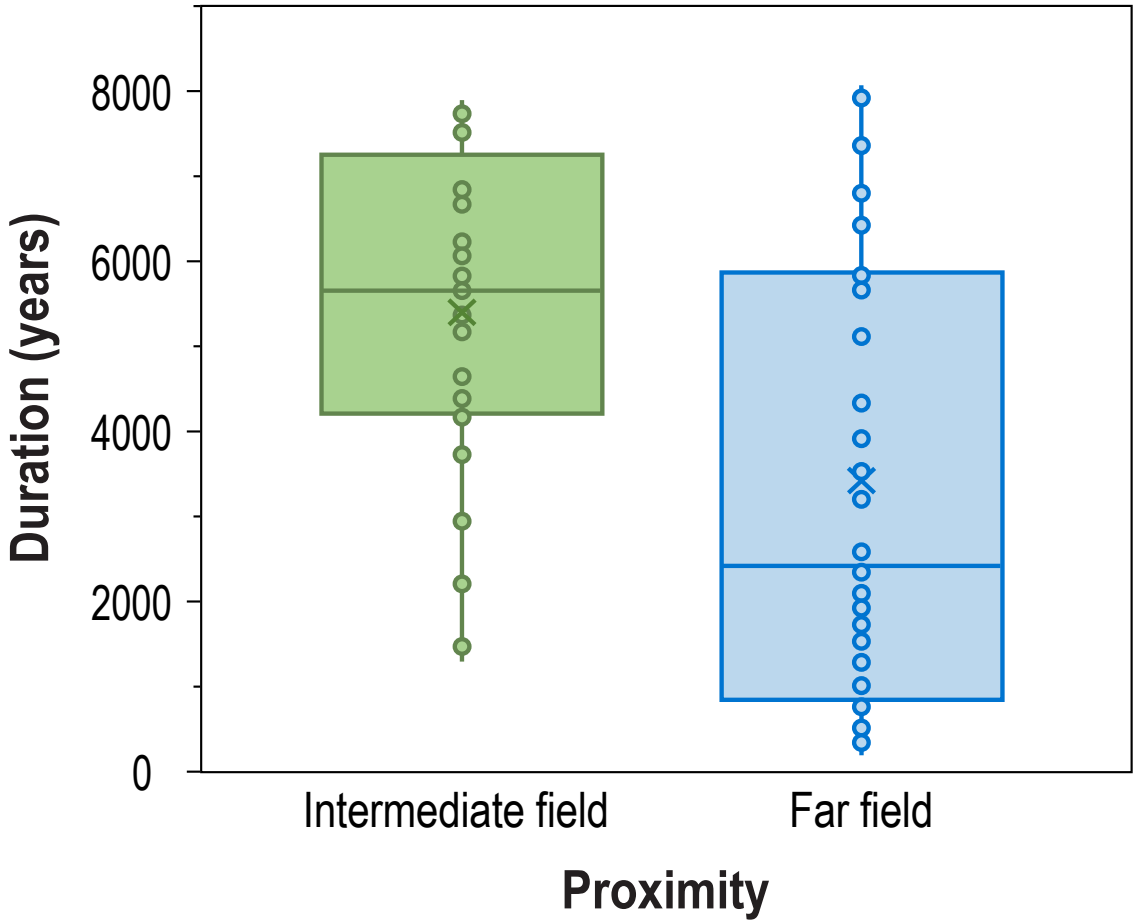

Fig S3. Mangrove duration (years) varies according to proximity to the Laurentide ice-sheet (P<0.001; Table S1). Vertical bar within each box represents the median and cross represents the mean for Intermediate-field locations (n=41) and Far-field locations (n=53).

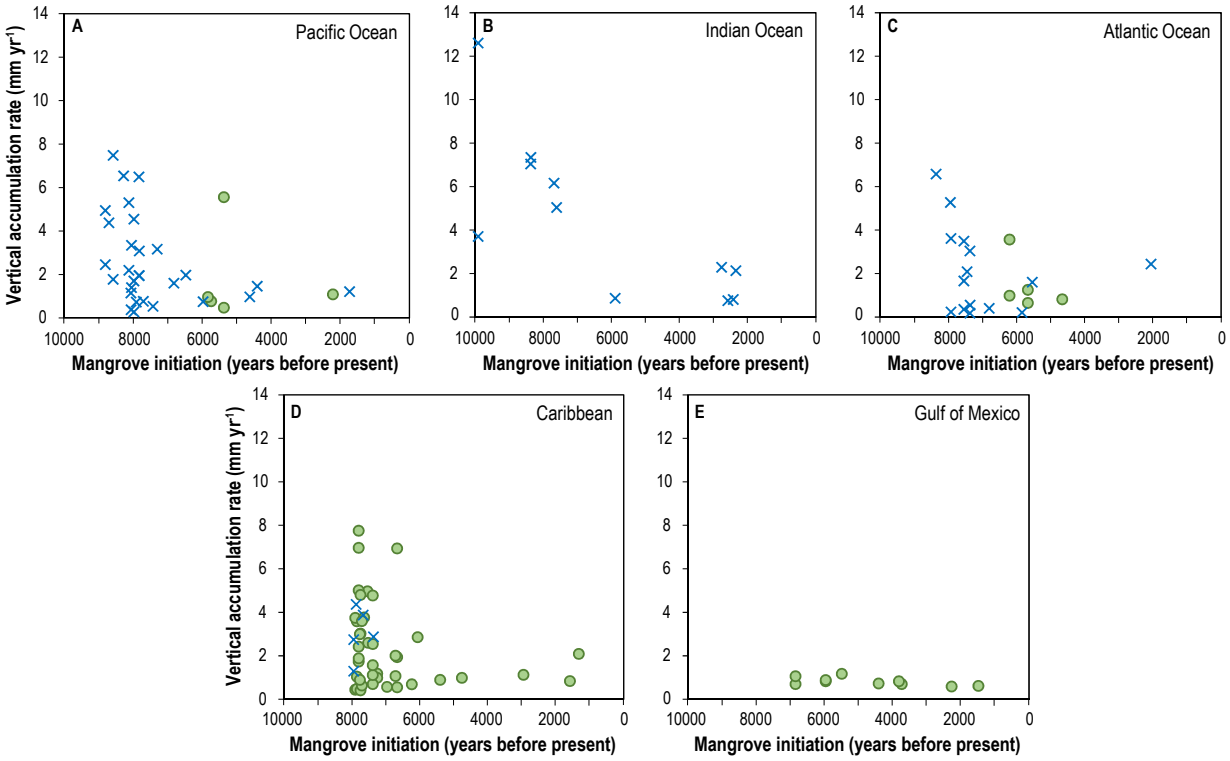

Fig S4. Mangrove initiation by ocean basin. Scatterplots of mangrove initiation (years before present) versus vertical accumulation rate (mm yr^{-1}) for intermediate (open circles) and far-field (crosses) locations among the Pacific Ocean (a), Indian Ocean (b), Atlantic Ocean (c), Caribbean (d) and Gulf of Mexico (e).

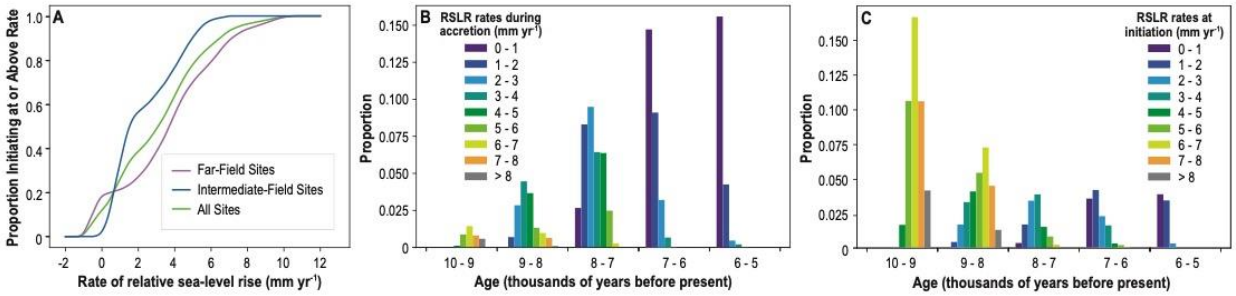

Fig S5. Details of probabilistic analysis of mangrove accretion conditional upon rates of RSLR. (A) Cumulative distribution function (cdf) of rates of RSLR during mangrove initiation for far-field, intermediate-field, and all sites. Histograms of RSLR rates during all time intervals of mangrove accretion (B) and during initiation of mangrove accretion (C) over each millennium (binned by 1 mm yr^{-1}).

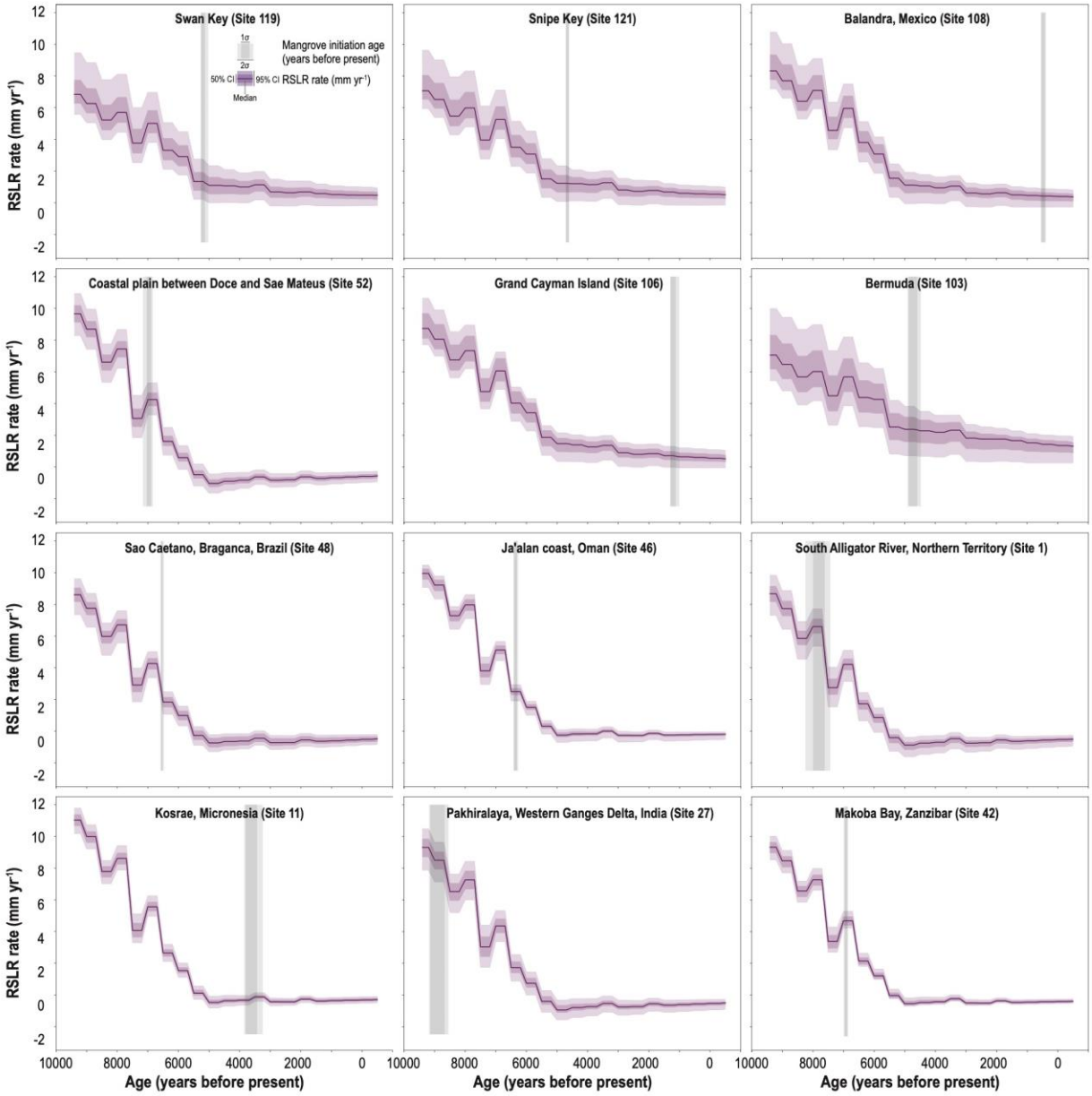

Fig S6. Examples of RSLR rates with uncertainties (50 and 95 confidence intervals) at selected sites predicted by the glacio-isostatic adjustment model. The grey bars represent the ages with uncertainties (1 and 2σ) during which initiation of mangrove accretion occurred.

5

Table S1.

Summary of statistical analysis of mangrove accretion rate and initiation: A) Generalised linear model (GLM) (Poisson distribution and log link function) testing whether mangrove duration (count of years mangrove persisted in situ) varies among proximity zones (intermediate vs far-field locations), including mangrove initiation date (cal yr BP) as a covariate. B) GLM (Gaussian distribution and identity link function) testing whether geomorphic setting (barrier estuarine, riverine estuarine, tidal estuarine, calcareous, and marine embayment), proximity to former ice sheets (intermediate- versus far-field), and tidal range (microtidal, mesotidal, and macrotidal) have significant effects on vertical accretion rates. C GLM (Gaussian distribution and identity link function) testing whether RSLR has a significant effect on vertical accretion rates.

A.

	Mean	**P-value**	**2.5th percentile**	**97.5th percentile**
Intercept	7.9	<0.001	7.887	7.912
proximity (intermediate, far field)	-0.595	<0.001	-0.602	-0.588
mangrove initiation (cal yrs BP)	1.14×10^{-4}	<0.001	1.123×10^{-4}	1.160×10^{-4}

B.

		Mean	**P-value**	**2.5th percentile**	**97.5th percentile**
Intercept		1.6483	0.004	0.516	2.781
Geomorphic Settings	calcareous	0.2562	0.636	-0.806	1.318
	marine embayment	-0.7628	0.196	-1.919	0.394
	riverine estuary	0.6779	0.310	-0.632	1.988
	tidal estuary	-0.7672	0.398	-2.548	1.014
tidal range		0.2909	0.465	-0.490	1.071
proximity (intermediate, far field)		0.8688	0.099	-0.165	1.902

C.

	Mean	**P-value**	**2.5th percentile**	**97.5th percentile**
RSLR rate	1.045	<.0.001	0.863	1.227

Intercept	1.311	<.0.001	0.977	1.645
Coefficient of Determination:	**0.517**			

Table S2.
Posterior probabilities of mangrove initiation when RSLR exceeds particular based on analysis of all sites in the database. For example, we found it was very likely (>90% probability, uncertainty interval (UI): 87.8% – 92.1%) that mangroves were unable to initiate sustained accretion when RSLR rates exceeded 6.1 mm yr^{-1}. This is equivalent to <10% probability of initiating with RSLR rates exceeding 6.1 mm yr^{-1}. We found it was extremely likely (>95% probability, UI 94.3% – 95.4%) that mangroves were unable to initiate sustained accretion when RSLR rates exceeded 7.6 mm yr^{-1} over all sites.

Rate (mm yr^{-1})	2.5th Percentile	5th Percentile	25th Percentile	Median	75th Percentile	95th Percentile	97.5th Percentile
0.1	98.4%	98.4%	98.5%	98.6%	98.6%	98.7%	98.7%
0.2	96.7%	96.8%	96.9%	97.1%	97.2%	97.3%	97.4%
0.3	94.9%	95.0%	95.2%	95.4%	95.5%	95.8%	95.8%
0.4	92.9%	93.0%	93.3%	93.5%	93.7%	94.0%	94.0%
0.5	90.7%	90.8%	91.2%	91.4%	91.7%	92.0%	92.1%
0.6	88.6%	88.7%	89.1%	89.4%	89.7%	90.0%	90.2%
0.7	86.7%	86.8%	87.2%	87.5%	87.8%	88.2%	88.3%
0.8	84.8%	84.9%	85.3%	85.7%	86.0%	86.5%	86.6%
0.9	83.1%	83.2%	83.6%	83.9%	84.3%	84.8%	85.0%
1.0	81.4%	81.6%	82.0%	82.4%	82.7%	83.3%	83.4%
1.1	79.9%	80.1%	80.6%	80.9%	81.3%	81.9%	82.1%
1.2	78.5%	78.7%	79.2%	79.6%	80.0%	80.6%	80.8%
1.3	77.2%	77.4%	77.9%	78.4%	78.8%	79.4%	79.6%
1.4	75.9%	76.1%	76.8%	77.2%	77.7%	78.3%	78.5%
1.5	74.8%	75.0%	75.7%	76.2%	76.6%	77.3%	77.5%
1.6	73.6%	73.8%	74.6%	75.1%	75.6%	76.3%	76.5%
1.7	72.4%	72.7%	73.5%	74.1%	74.6%	75.4%	75.6%
1.8	71.3%	71.6%	72.5%	73.1%	73.7%	74.5%	74.8%
1.9	70.3%	70.6%	71.5%	72.1%	72.8%	73.6%	73.9%
2.0	69.3%	69.5%	70.5%	71.2%	71.9%	72.8%	73.1%
2.1	68.2%	68.5%	69.5%	70.2%	70.9%	71.8%	72.2%
2.2	67.1%	67.4%	68.5%	69.2%	69.9%	70.9%	71.2%
2.3	66.0%	66.3%	67.4%	68.1%	68.9%	69.9%	70.2%
2.4	64.8%	65.1%	66.2%	67.0%	67.8%	68.9%	69.2%
2.5	63.5%	63.8%	65.0%	65.8%	66.7%	67.8%	68.1%
2.6	62.1%	62.5%	63.7%	64.6%	65.5%	66.7%	67.0%
2.7	60.7%	61.1%	62.4%	63.3%	64.2%	65.5%	65.8%
2.8	59.2%	59.6%	60.9%	61.9%	62.8%	64.1%	64.5%
2.9	57.6%	58.0%	59.4%	60.4%	61.4%	62.7%	63.2%
3.0	55.9%	56.4%	57.8%	58.8%	59.9%	61.3%	61.7%
3.1	54.2%	54.6%	56.1%	57.2%	58.3%	59.8%	60.2%
3.2	52.4%	52.8%	54.4%	55.5%	56.6%	58.2%	58.6%
3.3	50.5%	50.9%	52.6%	53.7%	54.9%	56.5%	57.0%
3.4	48.4%	48.9%	50.6%	51.8%	53.0%	54.7%	55.2%
3.5	46.3%	46.8%	48.5%	49.7%	51.0%	52.7%	53.2%
3.6	44.1%	44.6%	46.3%	47.6%	48.9%	50.6%	51.2%
3.7	41.7%	42.3%	44.1%	45.4%	46.7%	48.5%	49.1%

Rate (mm yr^{-1})	2.5th Percentile	5th Percentile	25th Percentile	Median	75th Percentile	95th Percentile	97.5th Percentile
3.8	39.5%	40.0%	41.8%	43.1%	44.5%	46.3%	46.9%
3.9	37.2%	37.7%	39.6%	40.9%	42.2%	44.1%	44.7%
4.0	34.9%	35.5%	37.3%	38.6%	40.0%	41.9%	42.5%
4.1	32.6%	33.2%	35.0%	36.3%	37.7%	39.6%	40.2%
4.2	30.4%	31.0%	32.8%	34.1%	35.4%	37.3%	37.9%
4.3	28.2%	28.8%	30.5%	31.8%	33.2%	35.0%	35.6%
4.4	26.1%	26.7%	28.4%	29.6%	31.0%	32.8%	33.3%
4.5	24.1%	24.7%	26.4%	27.6%	28.9%	30.6%	31.2%
4.6	22.3%	22.9%	24.5%	25.6%	26.9%	28.6%	29.1%
4.7	20.6%	21.2%	22.8%	23.9%	25.1%	26.7%	27.2%
4.8	19.1%	19.5%	21.1%	22.2%	23.4%	24.9%	25.4%
4.9	17.6%	18.1%	19.6%	20.6%	21.7%	23.2%	23.7%
5.0	16.2%	16.7%	18.2%	19.2%	20.2%	21.7%	22.1%
5.1	15.0%	15.5%	16.9%	17.8%	18.8%	20.3%	20.7%
5.2	13.9%	14.3%	15.7%	16.6%	17.6%	18.9%	19.3%
5.3	12.9%	13.3%	14.6%	15.5%	16.5%	17.8%	18.1%
5.4	12.0%	12.4%	13.7%	14.6%	15.5%	16.8%	17.1%
5.5	11.3%	11.7%	12.9%	13.8%	14.6%	15.9%	16.2%
5.6	10.6%	11.0%	12.2%	13.0%	13.9%	15.1%	15.4%
5.7	10.0%	10.3%	11.5%	12.3%	13.2%	14.4%	14.7%
5.8	9.4%	9.8%	10.9%	11.7%	12.5%	13.7%	14.1%
5.9	8.9%	9.2%	10.3%	11.1%	11.9%	13.1%	13.4%
6.0	8.4%	8.7%	9.8%	10.5%	11.3%	12.4%	12.8%
6.1	7.9%	8.2%	9.2%	10.0%	10.8%	11.9%	12.2%
6.2	7.5%	7.8%	8.8%	9.5%	10.2%	11.3%	11.6%
6.3	7.2%	7.4%	8.3%	9.0%	9.7%	10.8%	11.1%
6.4	6.8%	7.1%	7.9%	8.6%	9.2%	10.3%	10.6%
6.5	6.5%	6.7%	7.5%	8.1%	8.8%	9.7%	10.0%
6.6	6.2%	6.4%	7.1%	7.7%	8.3%	9.2%	9.5%
6.7	5.9%	6.1%	6.7%	7.3%	7.8%	8.7%	9.0%
6.8	5.7%	5.8%	6.4%	6.9%	7.4%	8.3%	8.5%
6.9	5.4%	5.6%	6.1%	6.5%	7.0%	7.8%	8.0%
7.0	5.3%	5.4%	5.8%	6.2%	6.7%	7.4%	7.6%
7.1	5.1%	5.2%	5.6%	5.9%	6.4%	7.1%	7.3%
7.2	5.0%	5.1%	5.4%	5.7%	6.1%	6.7%	6.9%
7.3	4.9%	5.0%	5.2%	5.5%	5.8%	6.4%	6.6%
7.4	4.8%	4.9%	5.1%	5.3%	5.6%	6.1%	6.3%
7.5	4.7%	4.8%	4.9%	5.1%	5.4%	5.8%	6.0%
7.6	4.6%	4.7%	4.8%	4.9%	5.2%	5.6%	5.7%
7.7	4.5%	4.5%	4.7%	4.8%	5.0%	5.3%	5.5%
7.8	4.4%	4.4%	4.6%	4.7%	4.8%	5.1%	5.2%
7.9	4.3%	4.3%	4.4%	4.5%	4.7%	4.9%	5.0%
8.0	4.1%	4.2%	4.3%	4.4%	4.5%	4.7%	4.9%
8.1	4.0%	4.1%	4.2%	4.3%	4.4%	4.6%	4.7%
8.2	3.9%	3.9%	4.1%	4.2%	4.3%	4.4%	4.5%
8.3	3.7%	3.8%	3.9%	4.1%	4.2%	4.3%	4.4%

Rate (mm yr^{-1})	2.5th Percentile	5th Percentile	25th Percentile	Median	75th Percentile	95th Percentile	97.5th Percentile
8.4	3.6%	3.6%	3.8%	3.9%	4.0%	4.2%	4.2%
8.5	3.4%	3.5%	3.7%	3.8%	3.9%	4.1%	4.1%
8.6	3.3%	3.4%	3.5%	3.7%	3.8%	3.9%	4.0%
8.7	3.1%	3.2%	3.4%	3.5%	3.7%	3.8%	3.8%
8.8	3.0%	3.0%	3.2%	3.4%	3.5%	3.6%	3.7%
8.9	2.8%	2.8%	3.0%	3.2%	3.3%	3.5%	3.5%
9.0	2.6%	2.6%	2.9%	3.0%	3.2%	3.3%	3.3%
9.1	2.4%	2.4%	2.7%	2.8%	3.0%	3.1%	3.2%
9.2	2.2%	2.3%	2.5%	2.6%	2.8%	2.9%	3.0%
9.3	2.0%	2.1%	2.3%	2.4%	2.6%	2.7%	2.8%
9.4	1.9%	1.9%	2.1%	2.3%	2.4%	2.6%	2.6%
9.5	1.7%	1.8%	2.0%	2.1%	2.2%	2.4%	2.4%
9.6	1.6%	1.6%	1.8%	1.9%	2.0%	2.2%	2.2%
9.7	1.5%	1.5%	1.7%	1.8%	1.8%	2.0%	2.0%
9.8	1.4%	1.4%	1.5%	1.6%	1.7%	1.8%	1.9%
9.9	1.3%	1.3%	1.4%	1.5%	1.6%	1.7%	1.7%
10.0	1.2%	1.2%	1.3%	1.4%	1.4%	1.5%	1.6%

Data S1. (separate file)

Core location, initiation and completion of mangrove soil development, and rates of vertical accretion.